Powder Technology 411 (2022) 117962

Contents lists available at ScienceDirect

Powder Technology

journal homepage: www.journals.elsevier.com/powder-technology

Application of coarse-graining for large scale simulation of fluid and particle motion in spiral jet mill by CFD-DEM

Lewis Scott [a], Antonia Borissova [a], Alberto Di Renzo [b], Mojtaba Ghadiri [a,*]

[a] School of Chemical and Process Science and Engineering, University of Leeds, Leeds LS2 9JT, UK
[b] DIMES Department, Università della Calabria, Via P. Bucci cubo 42C, 87036 Rende (CS), Italy

HIGHLIGHTS

- Coarse graining method is applied in the spiral jet mill using a CFD-DEM framework.
- Particle and fluid motion is similar in the bed at smaller scales.
- Insufficient particles were present in the lean phase to model the original system.
- Temporal dissipated energy remained constant for low coarse grain numbers.

GRAPHICAL ABSTRACT

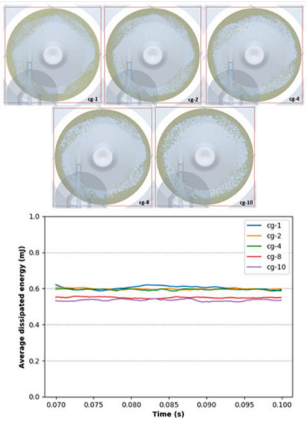

ARTICLE INFO

Keywords:
Coarse grain
Simulation
DEM
Spiral jet mill

ABSTRACT

Spiral jet milling is commonly used for size reduction of high value particulate solids, such as pharmaceutical ingredients, for which low contamination is critical. The mill utilises high-pressure gas nozzles to form an internal vortex and induce particle breakage through inter-particle collisions. Due to the centrifugal flow field, the particles can move radially inwards towards the mill centre and escape the mill only when their size is sufficiently reduced for the fluid drag to exceed the centrifugal force. Large particles move radially towards the outer wall and form a dense particle bed. The bed itself circulates in the milling chamber due to the induced effect of the inclined gas jets. In this study, we analyse the implementation of a coarse-graining (CG) approach on a coupled Computational Fluid Dynamic-Discrete Element Method simulation. Along with the actual particle size, four CG scale cases are compared (CG-2, CG-4, CG-8 and CG-10). To analyse the success of the approach in predicting the dynamics of fluid and particle motion, the characteristic features of the particle bed and fluid field, i.e. the fluid and particle velocity distributions and dissipated energy through particle collisions are analysed. There is good agreement between the original particle size and the two smallest scaled cases (CG-2, CG-4) for the above characteristics. However, modelling the lean phase is less successful, as there are fewer particles that reside there at any given time. There is also good agreement between these three cases in terms of dissipated

* Corresponding author.
E-mail address: M.Ghadiri@leeds.ac.uk (M. Ghadiri).

https://doi.org/10.1016/j.powtec.2022.117962
Received 12 July 2022; Received in revised form 12 September 2022; Accepted 16 September 2022
Available online 20 September 2022

energy through particle collisions. An average value for dissipated energy of 0.6 mJ is recorded for each of the three lowest cases. This proves beneficial for simulation time required, as the particle number is reduced 2-fold and 4-fold, respectively, and interparticle collision rate is reduced 60% each time.

1. Introduction

The spiral jet mill is a common item of size reduction equipment in industrial applications, where high value fine powders are required. It has a simple design and operation with a low level of contamination. Particle breakage is autogenous, as the mill has no moving parts and is operated using high-pressure gas nozzles. However, predicting an output particle size is difficult and currently it relies heavily on empirical knowledge, as both breakage and classification occur in the same chamber. The grinding nozzles induce an internal vortex, causing interparticle collisions that lead to particle breakage. Once the material has been sufficiently reduced in size, the gas overcomes the particles own inertia and drags them out of the mill.

More recently, simulation techniques have been used to model the underpinning mechanics inside the spiral jet mill. Teng et al. [1] using CFD-DEM were able to analyse the normal and tangential components of interparticle contacts, which indicated prevalent side-swipe collisions in their system. Rodnianski et al. [2], using only CFD, calculated the velocity ratio of the tangential and radial components of the fluid flow field, which could be used to determine classified particle size. However, they also concluded that CFD was not sufficient on its own, as it could not capture particle-fluid interactions. Brosh et al. [3] successfully simulated breakage using an in-house coupled CFD-DEM code. Although, they managed to decrease the time taken by removing ultrafine particles directly from the simulation, they found that the model was impractical due to the hardware available and time required. Dogbe [4] and Dogbe, et al. [5] analysed the collision frequency for different particle sizes and determined the size range of particles contributing most efficiently towards particle breakage. Bnà et al. [6] used a one-way coupled CFD-DEM approach to predict particle size classification and found good agreement with Dobson and Rothwell [7] cut size equation:

$$\delta_{cut} = \frac{3}{4}\frac{c_d \rho_g r_c}{\rho_p}\left(\frac{(v_{r,g})^2}{(v_{t,g})^2}\right) \tag{1}$$

where c_d is the particle drag coefficient, r_c is the classifier radius, $v_{r,\,g}$ is the radial component of the gas velocity, $v_{t,\,g}$ is the tangential component of the gas velocity, and ρ_g and ρ_p are the gas and particle densities, respectively. However, Bnà et al. [6] indicated that one-way coupling was only satisfactory at predicting the operation of a spiral jet mill if it operated as a classifier. Within their study, they also mainpulated the particle density/diameter relationship to artifically inflate the particle simulated size by reducing its density:

$$d_p = \frac{d_{p,fake} \bullet \rho_{p,fake}}{\rho_p} \tag{2}$$

where d_p and $d_{p,\,fake}$are the particle diameter and increased particle diameter, respectively, and ρ_p and $\rho_{p,\,fake}$ are the particle density and reduced density, respectively. They found an acceptable prediction for the translation components of particle motion. However, the scaling method was not able to predict the rotational motion of the artificially inflated particles. Scott et al. [8] analysed the role of hold-up on the fluid flow field and velocity distribution within the particle bed. Their results agreed with the experimental work of Luczak et al. [9].

Coarse-graining is a non-exact scaling method of scaling up the particle size, whilst maintaining the dynamics of the particle assemblage. Unlike individual particle scaling techniques, the particle size is not physically inflated. Instead, a group of particles is replaced by a single, larger particle with the same density as the small particles. The model is based on the assumption that the coarse-grain particles can statistically represent a cluster of the original system. This ensures that the change in particle number will not change the overall behaviour of the particle system, nor the fluid flow field when coupled with CFD. The drag force and other external forces are scaled so that forces acting on the coarse-grain particle match those of the group of original particles [10,11]. Coarse-graining has been successfully used to model CFD-DEM applications, such as pneumatic conveying [12], predicting dynamics of fluidised beds [13–16], flow patterns in a cyclone [11–17], powder dye deposition [18], large-scale three-phase-flow [19], and solids sedimentation in water [20]. Coarse-graining has also been used in molecular dynamics [21], particularly by Klein and Shinoda [22] to reduce 10 million atoms to 3265 particles. The benefit of applying coarse-graining to CFD-DEM models is a two-fold reduction in simulation time required. This is due to the combination of particle size enlargement, which in turn increases the time step and decreased number of particles present. Di Renzo et al. [23] point out the necessity to scale the fluid grid when applying coarse-graining to a particle system. Along with aiding convergence of the model, appropriate fluid cell scaling helps maintain the fluid-particle interactions for conserving interphase momentum exchange.

Coarse-graining offers an opportunity to reduce the simulation time required for predicting the complex fluid-particle relationship in the spiral jet mill. Unlike some scaling techniques, coarse-graining preserves mass and volume of the particle system in an effort to maintain the bulk material behaviour. In this study, the influence of coarse-graining on particle and fluid flow patterns in a spiral jet mill is explored following the method of Sakai [24] and without material scaling. In total, four scaled cases are compared to the system that contains unscaled particles. The particle velocity distribution and energy dissipated through collisions are analysed against the original particle systems. Particle breakage is not addressed in this study, and therefore, has not been implemented within the model.

2. Coarse-Graining in CFD-DEM framework

The coarse-grain (CG) methodology is applied to the DEM model [25] inside the CFD-DEM framework [26,27]. Particles of the same size and properties are then grouped together and replaced by a smaller number of larger particles, determined by the scaling factor selected. Grouping particles of a different size and averaging properties of the coarse-grain particle can lead to different translational or rotational motion once exposed to the fluid. To ensure the two systems are statistically analogous, three criteria must be met within the model: (i) the number of coarse-grain particles must be sufficient to statistically represent the original particle dynamics, so that bulk behaviour of the solids is not altered; (ii) the collisions between the coarse-grain particles must conserve momentum and energy, as they represent the collective result of many particles colliding; (iii) the number of coarse-grain particles must occupy the same fluid cell volume so that fluid-particle interaction is not changed [11].

The size of the coarse-grain particle is calculated from the number of particles it represents:

$$\varphi = \sqrt[3]{n_p} \tag{3}$$

where n_p is the number of particles replaced and φ is the scaling factor:

$$r_{cg} = \varphi r_o \tag{4}$$

and r_{cg} is the particle radius of the coarse-grain particle and r_o is the

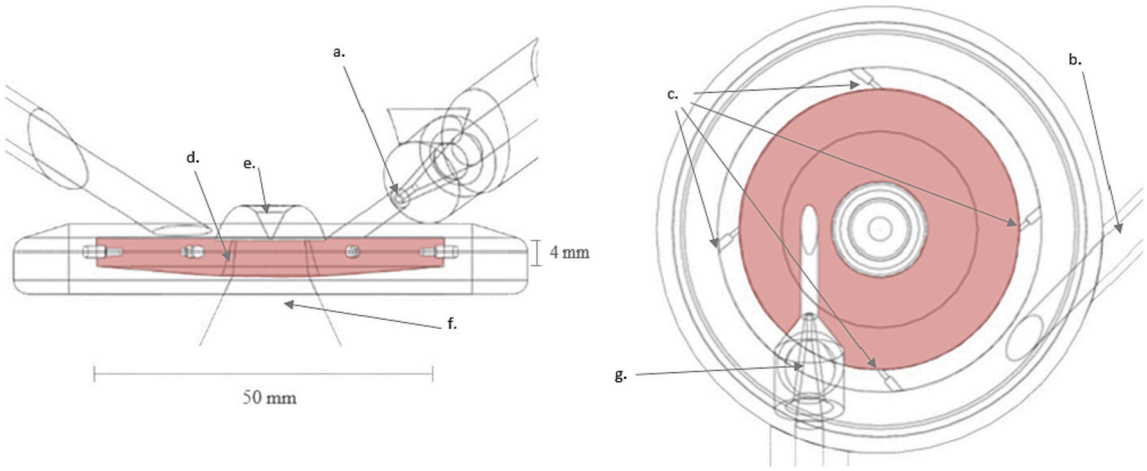

Fig. 1. An in-house made CAD drawing of Hosokawa Micron AS-50 mill. (a) feed gas nozzle, (b) grinding gas feed, (c) grinding gas nozzles, (d) classifier ring, (e) vortex finder, (f) mill exit pipe & (g) hopper section for solid feeding.

radius of the original particle. As the material density is kept constant, it follows that:

$$m_{cg} = \varphi^3 m_o \tag{5}$$

$$V_{cg} = \varphi^3 V_o \tag{6}$$

where m_{cg}, m_o and V_{cg}, V_o are the mass and volume of the coarse-grain particle and original particle, respectively.

To conserve the kinetic energy of the system, the velocity of the coarse-grain particle must equate to the average velocity of the group of original particles it represents:

$$\boldsymbol{v}_{cg} = \bar{\boldsymbol{v}}_o \tag{7}$$

where v_{cg} and $\bar{v}_o$ are the velocity of the coarse-grain particle and the group of original particles, respectively. According to Sakai [24], within the CFD-DEM framework, the equation for the momentum and impulse using spherical particles is simply scaled by φ^3:

$$m_{cg}\boldsymbol{v}_{cg} = \boldsymbol{F}_{f,cg} - V_{cg}\nabla P + \sum \boldsymbol{F}_{c,cg} + \boldsymbol{F}_{g,cg}$$

$$= \varphi^3 \boldsymbol{F}_{f,o} - \varphi^3 V_o \nabla P + \varphi^3 \sum \boldsymbol{F}_{c,o} + \varphi^3 \boldsymbol{F}_{g,o} \tag{8}$$

where V is the volume occupied by the particles in the fluid cell, P is the pressure, F_c is the contact force and F_g is the force of acceleration due to gravity. F_f is the fluid drag force and can be expressed as:

$$\boldsymbol{F}_{f,cg} = \frac{\beta_o}{1-\varepsilon}(\boldsymbol{u} - \boldsymbol{v}_{cg})V_{cg} = \varphi^3 \frac{\beta_o}{1-\varepsilon}(\boldsymbol{u} - \boldsymbol{v}_o)V_o$$

where β_o is the interphase momentum transfer coefficient of the original system, ε is a void fraction of the fulid cell and $\boldsymbol{u}$ is the fluid velocity.

In this work, a simplified version of coarse-graining has been applied, as the high-pressure fluid dominates the particle flow pattern. Therefore, the material properties of the particles have not been altered, nor have the contact mechanics.

3. Methodology

The simulated mill is based on the Hosokawa Micron AS-50 spiral jet mill using an in-house drawing made at the University of Leeds and is shown in Fig. 1. The main milling chamber is 50 mm in diameter and highlighted in red. The feed air/gas is supplied through the injector nozzle (a), acting as a Venturi eductor to entrain the feed particles from the funnel and into the milling chamber. However, in this work the particles are added directly into the chamber and not using the funnel to save computation time. Nevertheless, the simulation of fluid flow through the funnel is required as substantial air/gas is entrained through it. The particles are added into the main chamber at some radial mid-point, so that they are equally distanced from the chamber wall and classifier ring. A gas pipe (b) feeds pressurised air into the annular gas manifold, which in turn equally distributes the air into the milling chamber by means of four more nozzles (c); referred to as the grinding nozzles. The nozzles are equally spaced and set at 40° with respect to the tangent of the chamber wall at the centre point of the nozzle to encourage mixing and circulation of the particle bed. The manifold feeding the nozzles has been included in this study, as it was shown by Dogbe [4] to alter the fluid flow field compared to when it was not present. A particular feature of the spiral jet mills design is the classifier section at the centre of the mill. Due to the presence of the classifier ring (d), the air is forced upwards into a hemispherical chamber, whilst rotating fast in a vortex. The air then continues to circulate inside the chamber before being forced downwards by the vortex finder (e) out of the mill and into a catch pot (f). As mentioned previously, no particle is introduced into the mill using the hopper section (g), but its inclusion in the simulation is needed to account for the entrained air.

Table 1
Particle and fluid properties.

Mass of particles simulated (g)		1.0
Base particle size (μm)		100
Fluid feed pressure (kPa)		500
Fluid grinding pressure (kPa)		400
Coarse grain number (n_p)	Minimum fluid cell edge length (mm)	Particle number
1	0.4	233,213
2	0.56	117,057
4	0.71	58,664
8	0.9	29,397
10	1.0	23,550

In each case 1 g of material is simulated with a base particle size of 100 μm. The feed nozzle pressure is set at 5 barg, whilst the grinding gas pressure is 4 barg, in line with the industrial practice. As the coarse-grain number is increased, the size of the fluid cell is also increased to maintain the 40% particle-to-fluid cell volume, as suggested by Norouzi et al. [28]. Four coarse-grain numbers, n_p, 2, 4, 8 and 10, are analysed in the first study. Information regarding the mill is given in Table 1. For clarity in the discussion section, the original particle size is referred to as CG-1, with reference to the scaling factor. The total time allowed for each simulation is 0.1 s. Particles are added from $t = 0$ s using the standard EDEM™ factory until $t = 0.01$ s. A random distribution of *(0.75–1.0)r* is

Table 2
Fluid and particle parameters used in each simulation.

Phase	Parameter	Value
Fluid	Density, kg/m^3	Ideal gas law
	Viscosity, Pa s	1.8×10^{-5}
	Specific heat capacity (C_p), J/kg.k	1006.43
	CFD time step, μs	8–30
	Minimum cell edge length (no particles), mm	0.4
Particle	Density, kg/m^3	1500
	Shear modulus, MPa	10
	Poisson's ratio	0.25
	Coefficient of restitution	0.5
	Coefficient of static friction	0.5
	Coefficient of rolling friction	0.01
	DEM time step, μs	0.4–1.3

applied to particles on addition to the simulation. This will give a random distribution of size to the coarse-grain particle for a given n_p, thereby avoiding particle structuring within the dense bed. The particles were then allowed time to reach a pseudo-steady state before any results were recorded; typically this takes around 0.02–0.03 s. However, for results that are time dependant, a further 0.04 s was allowed before taking data.

The particle motion is calculated using EDEM™ 2019 (Altair, UK) and the fluid flow field is resolved by ANSYS Fluent 18.1. A four-way coupling scheme is adopted to record all fluid-particle interactions. To model the fluid flow field, the k-ε-RNG turbulence model with scalable wall functions is employed, along with the 'SIMPLE' pressure-velocity coupling scheme for the spatial discretisation. A tetrahedral mesh is used throughout the study and the minimum cell size is calculated based on the volume of an equilateral tetrahedron. Since EDEM™ uses spherical particles, the Morsi and Alexander [29] drag law is chosen for the particle-fluid drag calculations. Further fluid and particle parameters and properties are listed in Table 2. The correct scaling factor (φ) is provided to Fluent in each instance so that the drag force can also be appropriately scaled according to Eq. (8). The Hertz-Mindlin contact model is used by EDEM™ for calculating particle collisions [30].

4. Results

DEM results of the pattern of particle positions for the simulation of the original particle size and the four coarse-grains are shown in Fig. 2. There is no obvious change in the shape of the bed that has been caused by coarse graining. There is some variation in the bed depth as the particles approach the jet nozzles. However, this fluctuation in the solids distribution is typical during operation of the mill, as the material at the surface of the bed is not tightly bound and rotates around the mill more rapidly due to the influence of the jets. Yet there are noticeable differences amongst the cases when comparing the jet regions; i.e. particles ejected from the bed following a jet nozzle. In the CG-1 and CG-2 cases, the jet regions are occupied by a large number of particles, even though this area of the mill can be regarded as lean. However, for the three other cases; CG-4, CG-8 and CG-10, there are dramatically fewer particles travelling in the jet regions. This is of course intuitively expected as the number of particles in the system has decreased by the CG number used relative to the original case.

Fig. 3 depicts the modulus of the average particle velocity plotted as a function of the position on the x-y plane. To average the data, the particles are binned by position and then the mean velocity is calculated. The velocities range from 0 m/s (blue) to 30 m/s (red). The light-blue/teal colour represents the bed surface, which undulates due to the influence of the jets. Particles are either accelerated out of the bed or sheared across the top of the bed, before building up behind the next jet nozzle. Overall each case has produced a similar heat map, as each region of the mill has a similar average velocity. Particles in the bed travel at a velocity just above 0 m/s to 7 m/s, whilst particles in the jet regions at a velocity between 7 and 20 m/s. Very few particles were captured travelling in the lean region close to the centre of the mill due to their size. Noticeably, the square shape at the centre of each image is governed by the jets, as particles are projected along the jet axes.

Interestingly, the jet regions in the CG-10 case all have a lower

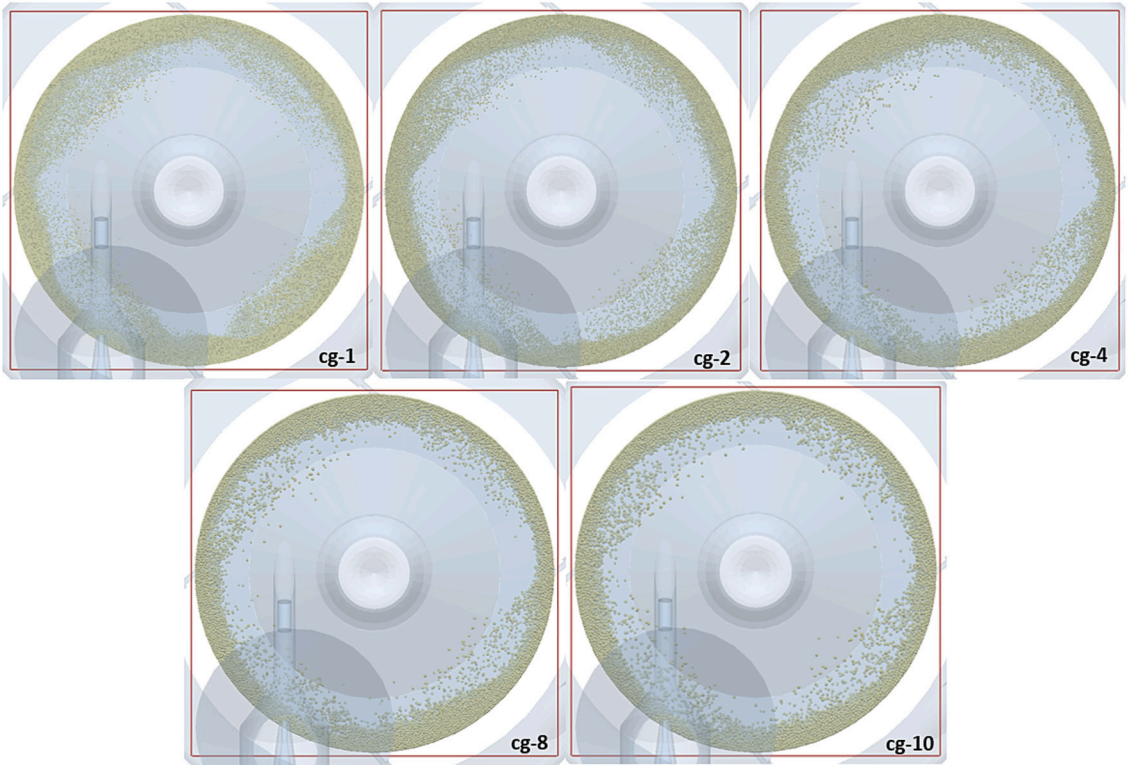

Fig. 2. Images of the DEM simulations at $t = 0.1$ s, showing particles in the mill chamber.

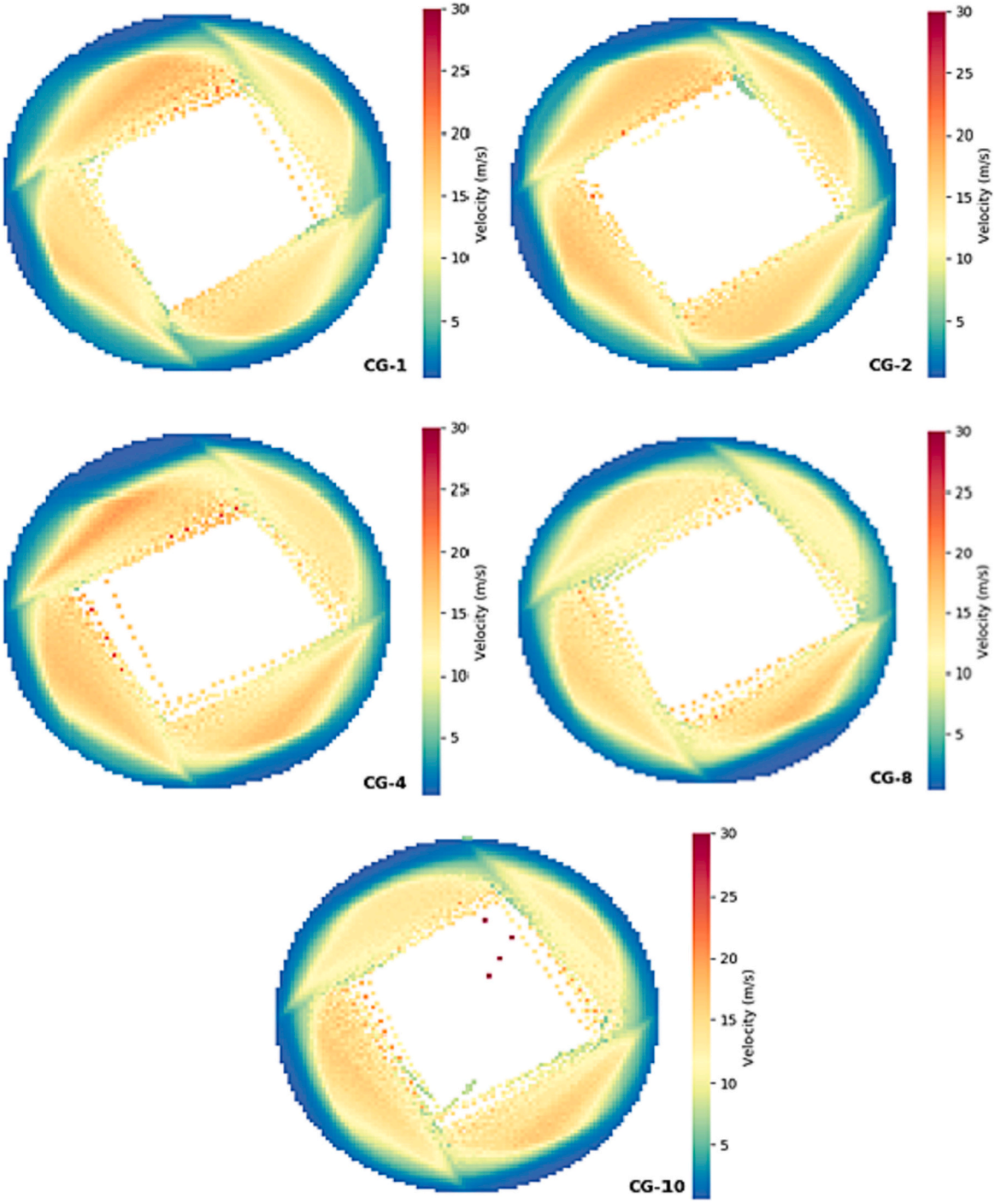

Fig. 3. Heat map of average particle velocity (m/s) in the milling chamber with respect to the x-y position. Data recorded from 0.07 to 0.1 s.

velocity when compared to each of the other cases, except a few particles in the lean phase. Therefore, it is concluded that this must be a consequence of coarse graining. Since the velocity has decreased, the particle number can no longer be representative of the original (CG-1) particle number.

In Fig. 4, each of the fluid flow fields can be seen. The velocity is plotted from blue to red colour, representing from 0 to 120 m/s, respectively. It has been capped at 120 m/s to increase the visibility of the flow patterns in various sections of the mill to view the boundaries of fluid that exist between the dense and lean phases. It can be seen that there is no significant change in the colour profiles at any given position in the mill amongst all the images. Furthermore, the lengths of the jets, denoted in red, do not vary in size. It can therefore be deducted that the changes in particle size and number are not adversely affecting the jet penetration and that the air has no easier path from the wall to the centre, even though the particle size has been increased. There is some minor variation in colour (light blue) directly behind each jet and in the top-left image; one of the jets has not penetrated through the bed. However, this can be attributed to localised build-up in particles that will naturally vary with time.

The particle system kinetic energy for each case is presented in Fig. 5. Initially, the energy of the particles is 0 mJ, at time $t = 0.0$ s, as the particles are placed into the mill with zero velocity. However, the particles quickly accelerate due to the high-pressure jets. The kinetic energy

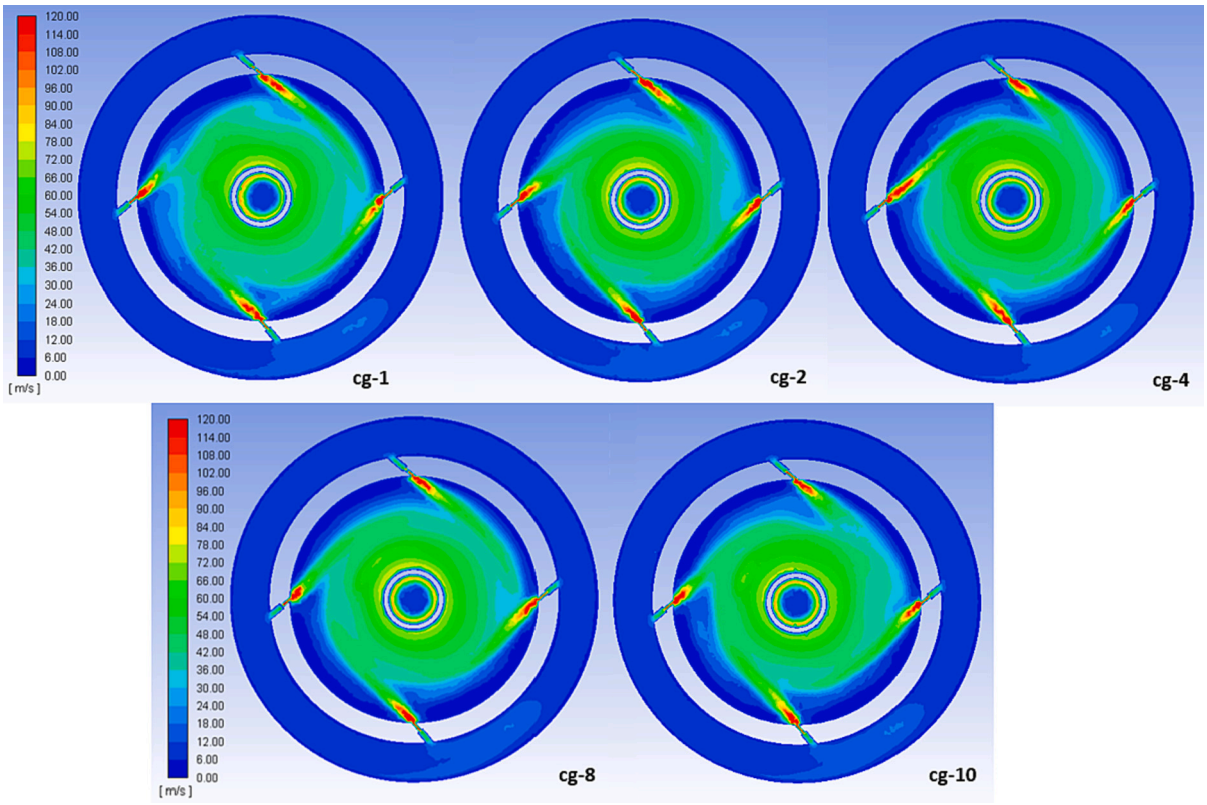

Fig. 4. Images of each corresponding fluid velocity field to its related particle system at time $t = 0.1$.

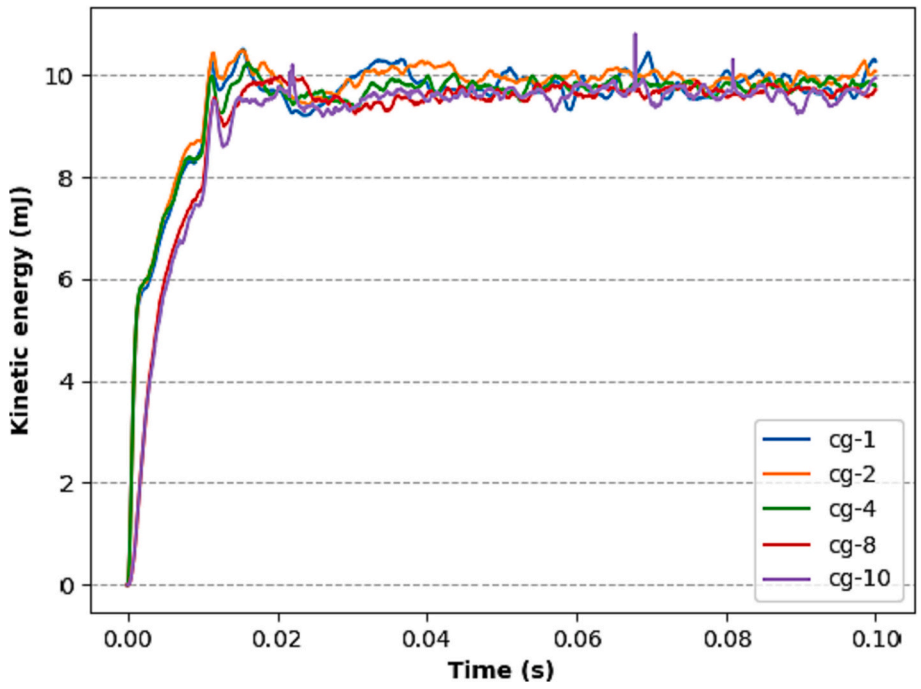

Fig. 5. Change in kinetic energy of the particle system for each coarse-grain number studied.

rapidly increases reaching an asymptotic value once the particle bed has formed and system has stabilised. The fluctuations recorded in each of the profiles are due to the rotation of the bed and ejection of material by the jets. Overall, the five cases achieve a similar asymptotic value once the system has stabilised, even though the particle number has been decreased ten folds. The agreement between the five profiles implies that both the particles and the fluid drag forces have been appropriately scaled, and the fluid cell loading has been maintained.

By plotting the particle velocity as a function of the radial distance from the outer wall, it can be seen where the different cases deviate. Fig. 6 is constructed using the radial distance of all the particles in the milling chamber. The values are binned by their x-y coordinates and

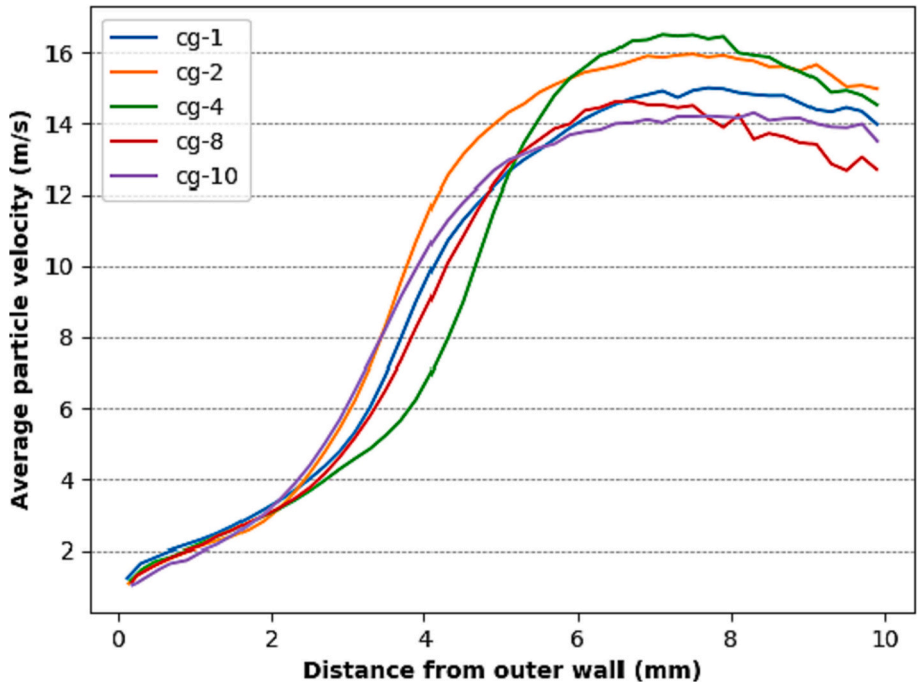

Fig. 6. Profile of particle velocity magnitude as a function of distance from the outer wall for each coarse-grain number studied from time 0.07 s to 0.1 s.

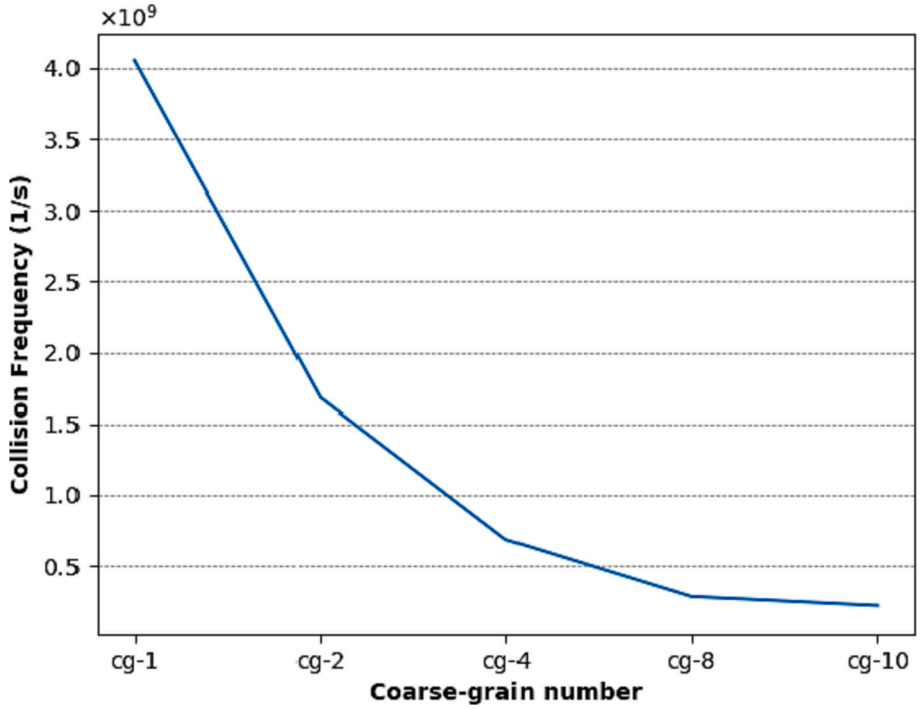

Fig. 7. Average calculated collision frequency from $t = 0.07$ s to $t = 0.1$ s for each coarse grain number studied.

modulus of the velocity is calculate for each bin. It can be seen that overall there is a good agreement amongst the profiles of the five cases up until around 3 mm. This distance signifies the average height of the bed. From this point, some of the cases start to deviate. The case with the largest difference is the CG-4 case. The case under-predicts the velocity of particles in the jet regions and over-predicts particle velocity in the lean phase. The under-estimation of particle velocity in the jet region may be due to the large number of particle build-up behind the jet at the 12 o'clock position. Averaging the particle velocities in the mill should reduce variation in bed height, but it can be seen in Fig. 3 that the CG-4 case appears to be highly unsymmetrical in particle distribution of the particle bed. The fluid field itself is unsymmetrical, due to the feed nozzle jet and entrained air, and may have caused particles to behave this way. However, it could also signify coarse-graining is failing to predict the particle velocity in the lean region.

The CG-2 case seems to over-predict the particle velocity at all radial positions outside the bed region. In Fig. 3, it can be seen that the particle distribution is largely even in all corresponding places of the milling

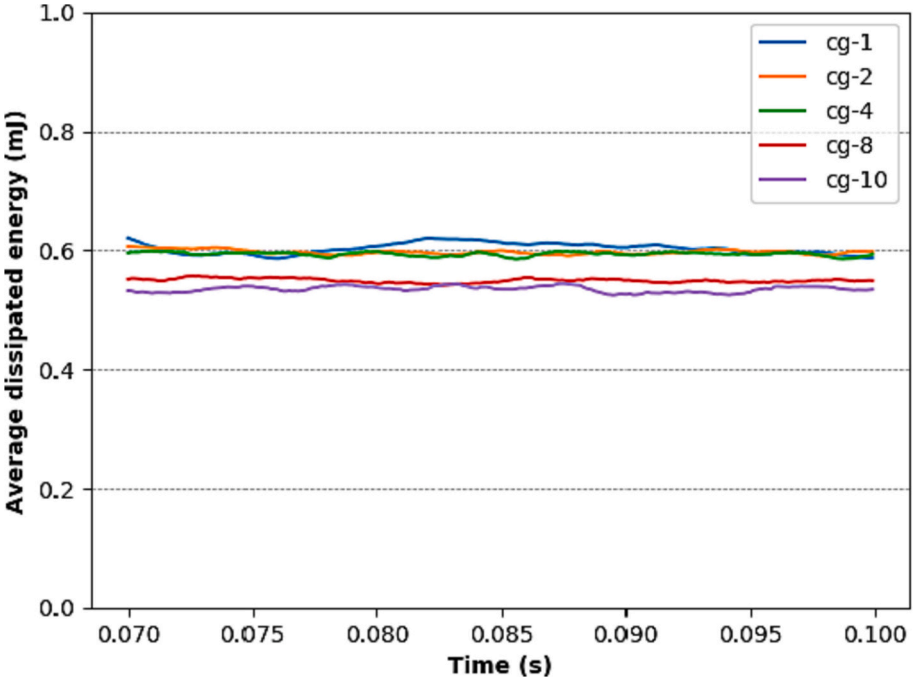

Fig. 8. Energy dissipated through collisions from time 0.07 s to 0.1 s for all cases.

chamber. As discussed, this effect will be beneficial for gas delivery, as the jet fluid energy is better utilised. Hence, higher particle velocities are produced in the jet and lean regions.

It is interesting to note that it is the CG-8 and CG-10 cases that agree with the original (CG-1) particle system in the lean region. However, for all cases, the data become unreliable and none of the coarse grain cases will realistically be able to model the lean phase of the mill. This is because beyond the jet regions the particle number drops significantly. Yet, this is less significant in the spiral jet mill, as most of the energy dissipation occurs within the top layers of the bed and close to the jets, where the particle phase is still dense [8,9,28].

In Fig. 7, the average collision frequency is shown. As expected, when the coarse-grain number increases, the number of collisions occurring between coarse-grain particles decreases substantially. This is because when a CG particle collides with another it corresponds to all original particles that are represented colliding simultaneously. The collision frequency is plotted against the coarse-grain number, for all collisions occurring between 0.07 s – 0.1 s. From CG-1 to CG-2, the number of particles roughly halves due to the random addition of particles. However, the number of collisions decreases by approximately 60%. This same decrease in collision frequency occurs once the coarse-grain number is increased from 2 to 4 and 4 to 8. The decrease in particle collision can be attributed to the increase in the mean-free length between successive collisions occurring.

The decrease in particle collisions is also substantial in terms of computational overhead required, as a large proportion of each time step in the DEM framework is related to contact detection and calculating collisions. The hardware used in this study is an Intel Xeon 2.6 GHz processor with 40 cores and 64 GB of RAM. The CG-1 case took around 72 h of simulating time, whereas the CG-4 took around 48 h and CG-10 less than 24 h.

Finally, the dissipated energy through particle-particle and particle-wall collisions is presented in Fig. 8. The dissipated energy is recorded for each time step and the mean value has been presented to improve readability of the results. There is good agreement between the CG-1, CG-2 and CG-4 profiles, even though the number of particles present has been halved and quartered respectively, when compared to the CG-1 case. However, the CG-8 and CG-10 profiles present an overall decrease in the value for energy dissipated. The most likely explanation for this deviation in the dissipated energy is from the underestimation in particle velocity in the lean phase and at boundaries. This decrease in the dissipated energy appears small; however, it still signifies that the assumption that coarse-grain particles are statistically analogous to the original particle size no longer holds true. Therefore, using large coarse-grain numbers may not be possible in the spiral jet mill given the different particle flow regimes.

5. Conclusions

The coarse grain (CG) method was applied within a coupled CFD-DEM simulation of a spiral jet mill to model the behaviour of the particles and to assess its validity/ applicability. Four CG numbers were investigated (2, 4, 8, 10) and compared against the original system of particles. Each system was first analysed qualitatively by investigating the shape of the bed and the accompanying fluid field. There was good agreement between all cases and the shape of the bed did not change, even though there was a decreasing number of larger particles. Furthermore, there was no noticeable change in the fluid velocity field. There was some minor localised fluctuations in the velocity profiles; however, this was attributed to normal particle build-up behind the jets. There was a noticeable difference in the time required, as the CG number was increased. This is due to the combination of particle size increasing and particle number decreasing.

To ensure that the particle system had reached a pseudo-steady state, the kinetic energy of the system was monitored and allowed to reach an asymptotic level before any data were taken for quantitative analysis. It was shown that the particle velocity of the dense bed regions compared well to one another for each scaled case against the original particle system. However, as the profiles extended radially inwards, they became more dissimilar with greater fluctuation. It was discussed that at a distance of 3 mm from the wall, the CG model may no longer hold valid as the original particle system is under represented in terms of dynamic behaviour. However, this finding may not affect the use of CG model in the analysis of particle dynamics in the spiral jet mill, as milling predominantly occurs at the surface of the bed and within its shearing layers, as indicated by spatial pattern of the dissipated energy.

Finally, the collision data were analysed. It was found that even though the interparticle collision rate had decreased significantly, due to the decreasing number of particles, the average rate of energy dissipation had remained constant between the original case and the smallest two CG numbers (CG-2 and CG-4). However, the increasing the CG number further led to a decrease in the average rate of dissipated energy for each particle system. This leads to the conclusion that whilst coarse graining is useful for scaling particle systems, it may be limited to what is achievable in the case of the spiral jet mill, given the constraint of modelling both lean and dense phases that exist.

CRediT authorship contribution statement

Lewis Scott: Methodology, Software, Visualization, Writing – original draft. **Antonia Borissova:** Supervision, Writing – review & editing. **Alberto Di Renzo:** Conceptualization. **Mojtaba Ghadiri:** Supervision, Writing – review & editing.

Declaration of Competing Interest

The authors declare the following financial interests/personal relationships which may be considered as potential competing interests:

Lewis Scott reports financial support was provided by AstraZeneca PLC. Lewis Scott reports was provided by Engineering and Physical Sciences Research Council.

Data availability

The data that has been used is confidential.

Acknowledgements

This project is supported by the Engineering and Physical Sciences Research Council, UK, through the Centre of Doctoral Training for Complex Particulate Products and Processes (CDT CP^3) (EPSRC Grant EP/L015285/1), which forms a part of the doctoral studies in collaboration with AstraZeneca Ltd. The authors gratefully acknowledge their support and would also like to especially thank Ian Gabbott and Catherine Hallam for their project co-ordination. We are also thankful to Altair Engineering, Edinburgh, UK, for providing a special license for the EDEM software (DEM Solutions) for use in this work.

References

[1] S. Teng, P. Wang, Q. Zhang, C. Gogos, Analysis of fluid energy mill by gas-solid two-phase flow simulation, Powder Technol. 208 (2011) 684–693, https://doi.org/10.1016/j.powtec.2010.12.033.
[2] V. Rodnianski, N. Krakauer, K. Darwesh, A. Levy, H. Kalman, I. Peyron, F. Ricard, Aerodynamic classification in a spiral jet mill, Powder Technol. 243 (2013) 110–119, https://doi.org/10.1016/j.powtec.2013.03.018.
[3] T. Brosh, H. Kalman, A. Levy, I. Peyron, F. Ricard, DEM-CFD simulation of particle comminution in jet-mill, Powder Technol. 257 (2014) 104–112, https://doi.org/10.1016/j.powtec.2014.02.043.
[4] S.C. Dogbe, Predictive Milling of Active Pharmaceutical Ingredients and Excipients, PhD Thesis, The University of Leeds, 2017.
[5] S. Dogbe, M. Ghadiri, A. Hassanpour, C. Hare, D. Wilson, R. Storey, I. Crosley, Fluid-particle energy transfer in spiral jet milling, EPJ Web of Conferences 140 (2017) 7–10, https://doi.org/10.1051/epjconf/201714009040.
[6] S. Bnà, R. Ponzini, M. Cestari, C. Cavazzoni, C. Cottini, A. Benassi, Investigation of particle dynamics and classification mechanism in a spiral jet mill through computational fluid dynamics and discrete element methods, Powder Technol. 364 (2020) 746–773, https://doi.org/10.1016/j.powtec.2020.02.029.
[7] B. Dobson, E. Rothwell, Particle size reduction in a fluid energy mill, Powder Technol. 3 (1969) 213–217, https://doi.org/10.1016/0032-5910(69)80080-X.
[8] L. Scott, A. Borissova, A. Burns, M. Ghadiri, Influence of holdup on gas and particle flow patterns in a spiral jet mill, Powder Technol. 377 (2021) 233–243, https://doi.org/10.1016/j.powtec.2020.08.099.
[9] B. Luczak, R. Müller, C. Kessel, M. Ulbricht, H.J. Schultz, Visualization of flow conditions inside spiral jet mills with different nozzle numbers– analysis of unloaded and loaded mills and correlation with grinding performance, Powder Technol. 342 (2019) 108–117, https://doi.org/10.1016/j.powtec.2018.09.078.
[10] Y. Mori, M. Sakai, Visualization study on the coarse graining DEM for large-scale gas–solid flow systems, Particuology (2020), https://doi.org/10.1016/j.partic.2020.07.001.
[11] K. Chu, J. Chen, A. Yu, Applicability of a coarse-grained CFD–DEM model on dense medium cyclone, Miner. Eng. 90 (2016) 43–54, https://doi.org/10.1016/J.MINENG.2016.01.020.
[12] M. Sakai, S. Koshizuka, Large-scale discrete element modeling in pneumatic conveying, Chem. Eng. Sci. 64 (2009) 533–539, https://doi.org/10.1016/J.CES.2008.10.003.
[13] M. Sakai, M. Abe, Y. Shigeto, S. Mizutani, H. Takahashi, A. Viré, J.R. Percival, J. Xiang, C.C. Pain, Verification and validation of a coarse grain model of the DEM in a bubbling fluidized bed, Chem. Eng. J. 244 (2014) 33–43, https://doi.org/10.1016/j.cej.2014.01.029.
[14] M. Girardi, S. Radl, S. Sundaresan, Simulating wet gas–solid fluidized beds using coarse-grid CFD-DEM, Chem. Eng. Sci. 144 (2016) 224–238, https://doi.org/10.1016/J.CES.2016.01.017.
[15] L. Lu, K. Yoo, S. Benyahia, Coarse-grained-particle method for simulation of liquid−solids reacting flows, Ind. Eng. Chem. Res. 55 (2016) 10477–10491, https://doi.org/10.1021/acs.iecr.6b02688.
[16] A. Nikolopoulos, A. Stroh, M. Zeneli, F. Alobaid, N. Nikolopoulos, J. Ströhle, S. Karellas, B. Epple, P. Grammelis, Numerical investigation and comparison of coarse grain CFD – DEM and TFM in the case of a 1 MWth fluidized bed carbonator simulation, Chem. Eng. Sci. 163 (2017) 189–205, https://doi.org/10.1016/J.CES.2017.01.052.
[17] E.S. Napolitano, A. Di Renzo, F.P. Di Maio, Coarse-grain DEM-CFD modelling of dense particle flow in Gas–Solid cyclone, Sep. Purif. Technol. 287 (2022), 120591, https://doi.org/10.1016/J.SEPPUR.2022.120591.
[18] P.M. Widartiningsih, Y. Mori, K. Takabatake, C.Y. Wu, K. Yokoi, A. Yamaguchi, M. Sakai, Coarse graining DEM simulations of a powder die-filling system, Powder Technol. 371 (2020) 83–95, https://doi.org/10.1016/j.powtec.2020.05.063.
[19] K. Washino, E.L. Chan, T. Kaji, Y. Matsuno, T. Tanaka, On large scale CFD–DEM simulation for gas–liquid–solid three-phase flows, Particuology (2020), https://doi.org/10.1016/j.partic.2020.05.006.
[20] Z. Xie, Y. Shen, K. Takabatake, A. Yamaguchi, M. Sakai, Coarse-grained DEM study of solids sedimentation in water, Powder Technol. 361 (2020) 21–32, https://doi.org/10.1016/j.powtec.2019.11.034.
[21] V. Tozzini, Coarse-grained models for proteins, Curr. Opin. Struct. Biol. 15 (2005) 144–150, https://doi.org/10.1016/j.sbi.2005.02.005.
[22] M.L. Klein, W. Shinoda, Large-scale molecular dynamics simulations of self-assembling systems, Science 321 (2008) 798–800, https://doi.org/10.1126/science.1157834.
[23] A. Di Renzo, E.S. Napolitano, F.P. Di Maio, Coarse-grain DEM modelling in fluidized bed simulation: a review, Processes 9 (2021) 279, https://doi.org/10.3390/PR9020279.
[24] M. Sakai, How Should the Discrete Element Method Be Applied in Industrial Systems?: A Review †. ©2016 Hosokawa Powder Technology Foundation KONA Powder and Particle Journal No, 33, 2016, pp. 169–178, https://doi.org/10.14356/kona.2016023.
[25] P.A. Cundall, O.D.L. Strack, A discrete numerical model for granular assemblies, Géotechnique 29 (1979) 47–65, https://doi.org/10.1680/geot.1979.29.1.47.
[26] Y. Tsuji, T. Kawaguchi, T. Tanaka, Discrete particle simulation of two-dimensional fluidized bed, Powder Technol. 77 (1993) 79–87, https://doi.org/10.1016/0032-5910(93)85010-7.
[27] B.H. Xu, A.B. Yu, Numerical simulation of the gas-solid flow in a fluidized bed by combining discrete particle method with computational fluid dynamics, Chem. Eng. Sci. 52 (1997) 2785–2809, https://doi.org/10.1016/S0009-2509(97)00081-X.
[28] H. Norouzi, R. Zarghami, R. Sotudeh-Gharebagh, N. Mostoufi, Coupled CFD-DEM Modeling, John Wiley & Sons, Chichester, 2016.
[29] S.A. Morsi, A.J. Alexander, An investigation of particle trajectories in two-phase flow systems, J. Fluid Mech. 55 (1972) 193–208, https://doi.org/10.1017/S0022112072001806.
[30] C. Thornton, Applications of dem to process engineering problems, Eng. Comput. 9 (1992) 289–297, https://doi.org/10.1108/eb023867.